HIGH SPEED STRENGTH TESTING OF OPTICAL FIBER

G.S. GLAESEMANN, D.A. CLARK, T.A. HANSON, D.J. WISSUCHEK
Corning Incorporated, Corning, NY 14831

ABSTRACT

Optical fiber models for mechanical reliability require that the initial strength and crack growth parameters be measured. High speed testing allows one to investigate and model common high-speed processing events during fiber processing such as proof testing, coloring and cabling. In this study stressing rates ranging from $7x10^{-6}$ GPa/s to 1.5 TPa/s were accomplished using a universal testing machine, belt slide and pneumatic piston. When plotted in typical dynamic fatigue fashion the data shows curvature at the faster stressing rates. The presence of region II type crack growth is suggested as a possible explanation for this curvature. A multi-region crack growth model is used to extract crack growth parameters that are used to make comparisons with crack velocity results on bulk glass.

INTRODUCTION

Optical fiber strength degradation over long-term in-service lifetimes is modeled by extrapolating relatively short-term fatigue data to long time frames. The in-service portion of the fiber's lifetime occurs after several processing steps. It is now expected that reliability models for optical fiber incorporate the effect of proof testing on the strength distribution. Since proof testing is a high-speed event, the modeling of this event involves an extrapolation from typical fatigue data. It is assumed that the underlying crack growth model and crack growth parameters used in the in-service lifetime extrapolation hold for high speed processing events as well. Strength tests of proof stress level flaws on coated optical fiber have been performed at loading rates corresponding to those commonly found during high speed fiber processing.[1,2] These results are summarized in Figure 1 and indicate that the dependence of strength on loading rate is different for fast loading rates than slower rates.

High-speed strength testing of bulk soda-lime glass has been used for fundamental studies of the strength and fatigue behavior of flaws in glass.[3,4] Techniques for high-speed strength testing of proof stress level flaws in optical fiber have progressed to a point where the effects of subcritical crack growth on fiber strength are minimal. The purpose of this paper is to explore the fatigue behavior of flaws in optical fiber near the proof stress in an attempt at determining functional crack growth parameters for modeling high speed processing events.

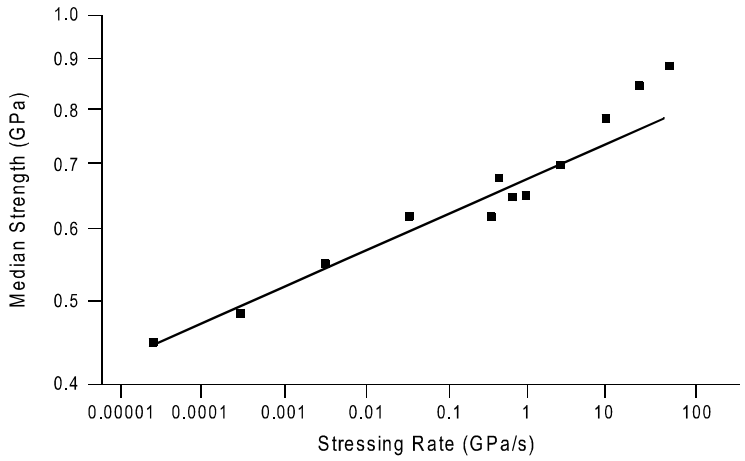

Figure 1. Optical Fiber Strength Over a Wide Range of Stressing Rates in Ambient Test Conditions from Reference 2.

EXPERIMENTAL PROCEDURE

Proof-Stress level flaws were obtained by abrading the fiber during the draw process before application of the coating. Draw-abraded fiber was used in this study because it is identical to standard fiber in composition and processing while providing a high density of flaws near the proof stress level. The abrasion process consists of contacting the fiber being drawn with another fiber below the draw furnace.[5] It is believed that this abrasion method produces surface flaws in silica optical fiber with little contact residual stress. This abrasion method yielded a typical Weibull modulus, m, of 21. The fiber used in this study was a standard single-mode silica-clad fiber coated with a standard dual-layer acrylate coating.

Three loading techniques were used to generate strength values over nearly eight decades of stressing rates. For the slower speed tests, 7×10^{-6} to 0.7 GPa/s (0.001 to 100 kpsi/s), a conventional universal testing machine$^{\alpha}$ was adapted with sixteen load cells and corresponding capstans. Thus, instead of the usual single fiber testing method, sixteen fibers could be tested in tension simultaneously. This greatly decreases the overall experimental time at the slower rates. A belt slide$^{\tau}$ was used to generate stressing rates ranging from 1 to 50 GPa/s (150 to 7000 kpsi/s). For the highest load rates, a pneumatic piston$^{\beta}$ with gas pressure levels ranging from 280 to 665 kPa (40 to 95 psi) were used to achieve stressing rates ranging from 365 to 1530

$^{\alpha}$ Instron Corp., Canton, MA.
$^{\tau}$ Hauser Linear Drive, Harrison City, PA.
$^{\beta}$ SMC, Indianapolis, IN

GPa/s (53,000 to 2.2x10^5 kpsi/s). A gauge length of 0.5 m was used for all tests. A small amount of slack in the fiber gauge length was introduced at the higher loading rates to allow the test device to reach its maximum speed before fiber loading.

Of primary importance to high speed testing is the mass of the fiber attachment system and the method of data acquisition. All tests on the belt slide and air piston were performed with two load cells in place, a conventional lightweight strain gauge load cell[χ] and a piezoelectric load cell.[δ] The piezoelectric load cell was chosen such that drift and resonant frequency problems were minimized for the range of failure times used in this study.

Fiber was attached to both load cells by carefully taping the fiber to a nylon screw that was threaded directly into the load cell. The total weight of the screw and tape was approximately 1 gram. Fiber pullout from the tape was not an issue since the maximum loads were sufficiently low with the abraded fiber.

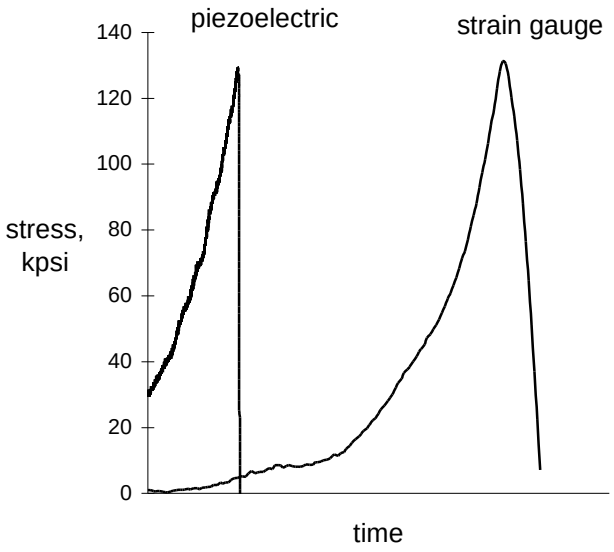

Figure 2. Loading curves for both load cell types at the fastest loading rate.[6]

The data acquisition rate for the strain gauge load cell at the highest speeds was 40,000 HZ. At the highest loading rate the failure times were on the order of 10^{-3} seconds; and therefore, the number of data points using this load cell were considerable. The signal from the piezoelectric load cell, on the other hand, was monitored at 5x10^6 HZ using a digital oscilloscope. This yielded several thousand data points per test at the highest speed. Figure 2 shows a typical loading curve for both load cells operating at the fastest loading rate from a previous study using the same technique.[6] The stressing rate was taken from the last 20% of the loading region.

At the fastest stressing rate there is concern that the load cell does not see the peak stress generated by the opposite “pulling” end of the fiber. A stress wave propagating through silica at approximately 5000 m/s may not reach the load cell before

---

[χ] Interface, Inc., Scottsdale, AZ.
[δ] Kistler Instrument Corp., Amherst, NY.

failure occurs. This concern was addressed by comparing the measured failure stress to that predicted by the fracture mirror radius. Good agreement was found.

Since most high speed processing events like proof testing are conducted immediately after drawing the fiber, testing was completed in the ambient environment of 22°C and 50% within a few days of drawing the fiber. Identical tests were also conducted in 100% RH at the same time as the ambient tests by using single fiber humidity chambers. A minimum of 15 specimens per loading rate was tested. Only failures in the gauge length were accepted. All fibers were preconditioned fiber in the test environment for a minimum of 24 hours before testing. For the high-speed tests on the belt slide and pneumatic piston specimens were removed from the preconditioning environment and loaded to failure in less than 30 seconds.

RESULTS AND ANALYSIS

The measured fatigue strengths for both the ambient and 100% RH test environments are summarized in typical “power law” fashion in Figure 3.

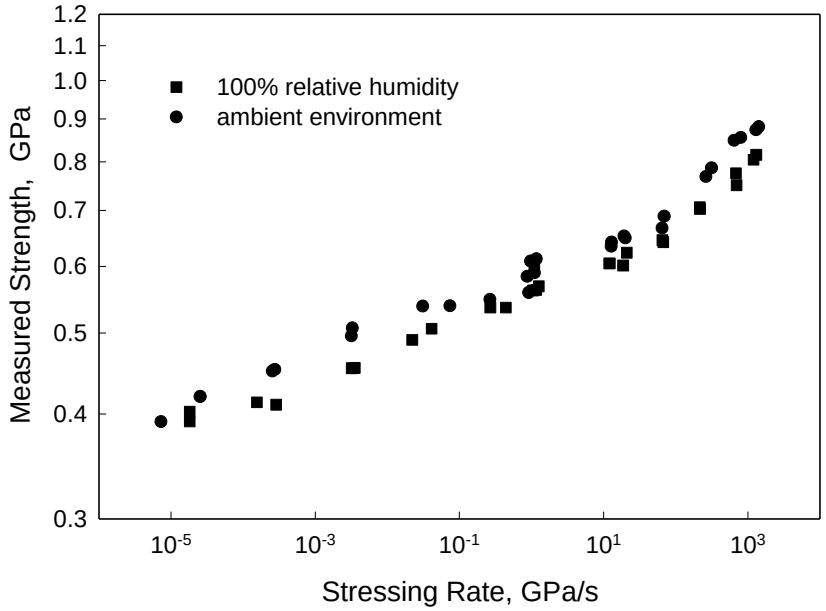

Figure 3. Dynamic Fatigue of Abraded Optical Fiber Measured in Ambient and 100%RH Environments.

The data points shown represent the median strength for an odd number of gauge length failures at a given stressing rate and the middle two data points for an even number of gauge length failures. The strengths obtained in the ambient

environment are approximately 5% higher than those measured in the wet environment. There is a clear non-linear dependence of strength on stressing rate for both environments.

Curvature at the faster stressing rates is clearly evident and is similar to what has been observed in two other studies.[1,3] In order to produce an engineering model for high speed processing events one must take into account the curvature in the fatigue behavior of proof test level flaws. Such curvature in the dynamic fatigue plot is consistent with the onset of transport rate limited stress-corrosion cracking commonly referred to as region II crack growth.[3] A multi-region crack growth model is used as a framework for modeling such behavior.

Region I and II crack velocity behavior can be simplistically modeled as two straight lines intersecting at $K_I/K_{IC} = r$ as shown in Figure 4.[7] The parameter "r" is the stress intensity factor where the crack velocity transitions from region I to region II. The crack velocity model can be written as,[1]

$$\frac{da}{dt} = A_1\left(\frac{K_I}{K_{IC}}\right)^{n_1} \quad \text{for } K_I \le rK_{IC} \text{ (region I)} \tag{1a}$$

$$\frac{da}{dt} = A_2\left(\frac{K_I}{K_{IC}}\right)^{n_2} \quad \text{for } K_I > rK_{IC} \text{ (region II)} \tag{1b}$$

where $A_1 = A_2 r^{(n_2 - n_1)}$.

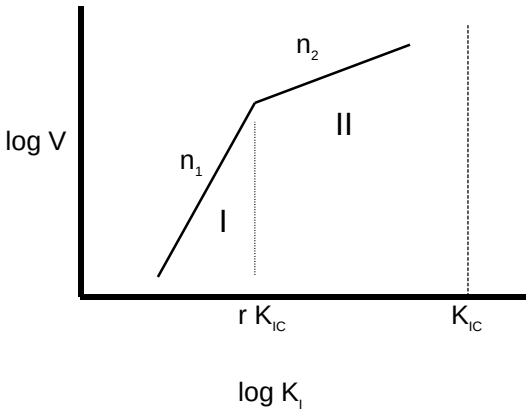

Figure 4. Schematic of the two-region power law crack velocity model.

Using conventional fracture mechanics theory Eq. (1) can be rewritten in strength degradation terms for a dynamic fatigue test,

$$S_i^{n_1-2} = S_r^{n_1-2} + \frac{s_r^{n_1+1}}{B_1(n_1+1)\dot{s}} \qquad \text{for crack growth through region I} \quad (2a)$$

$$S_r^{n_2-2} = s_f^{n_2-2} + \frac{s_f^{n_2+1} - s_r^{n_2+1}}{B_2(n_2+1)\dot{s}} \quad \text{for crack growth through region II} \quad (2b)$$

where S_i is the initial strength before loading, S_r and s_r are the strength and applied stress when $K_I/K_{IC} = r$ (i.e., $s_r/S_r = r$), s_f is the fatigue strength for stress rate, $\dot{s}$, $1/B_2 = A_2(n_2-2)/2(Y/K_{IC})^2$ and $B_1 = B_2 r^{n_1-n_2}(n_2-2)/(n_1-2)$.[ζ]

As the flaw is loaded it grows subcritically from the initial strength, S_i, down to strength S_r according to Eq. (2a). From there it transitions to region II growth starting at strength S_r and finally fails at strength s_f according to Eq. (2b). The crack growth parameters n_1, n_2, r, and B_2 are determined in an iterative fashion by minimizing the variability in the predicted initial strength, S_i, across all stressing rates. Once the crack growth parameters are determined, the predicted fatigue strength, s_f, can be plotted using Eq.(2). The curvature in the dynamic fatigue plot results from a reduced region I influence at the higher stressing rates.

Figure 5 shows the predicted initial strength, S_i, (open symbols) and predicted fatigue strength, s_f, (solid line) for both test environments. The crack growth parameters from this study are summarized in Table I.

Table I. Predicted Crack Growth Parameters from High Speed Testing of Abraded Optical Fiber.[ɜ]

	This Study ambient	This Study 100% RH
n_1	28	28
n_2	2.25	2.25
r	0.81	0.81
B_1 GPa^{2}s	1.86x10^{-7}	4.14x10^{-8}
B_2 GPa^{2}s	4.39x10^{-3}	9.78 x10^{-4}
A_1 m/s	0.187	0.840
A_2 m/s	8.25 x10^{-4}	3.70 x10^{-3}

[ζ] This corrects a mathematical error in reference 1 where B_1 was given as $B_1 = B_2 r^{n_1-n_2}(n_1-2)/(n_2-2)$.

[ɜ] K_{IC} = 0.75 MPa m1/2 (Reference 8) and Y =0.73$\sqrt{p}$ (Reference 9).

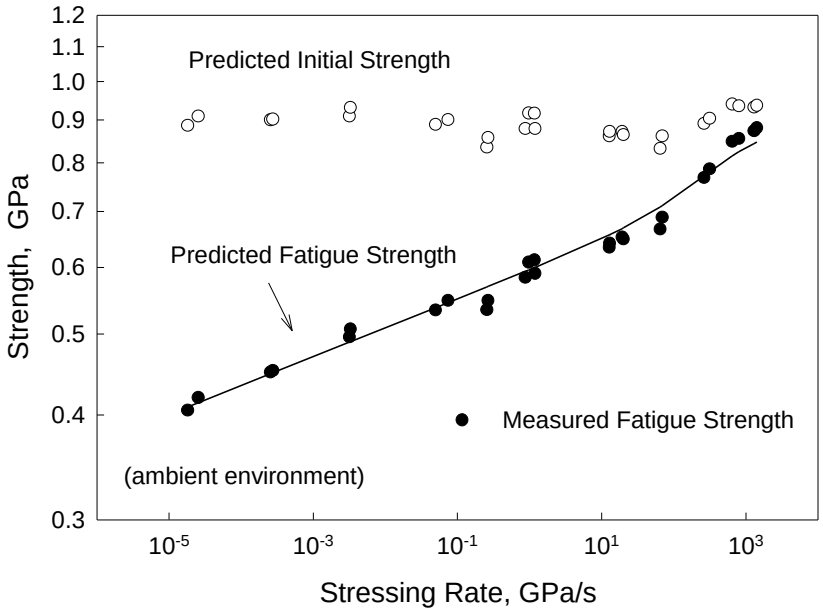

Figure 5a. Predicted Initial and Fatigue Strength for Abraded Optical Fiber Tested in Ambient Conditions.

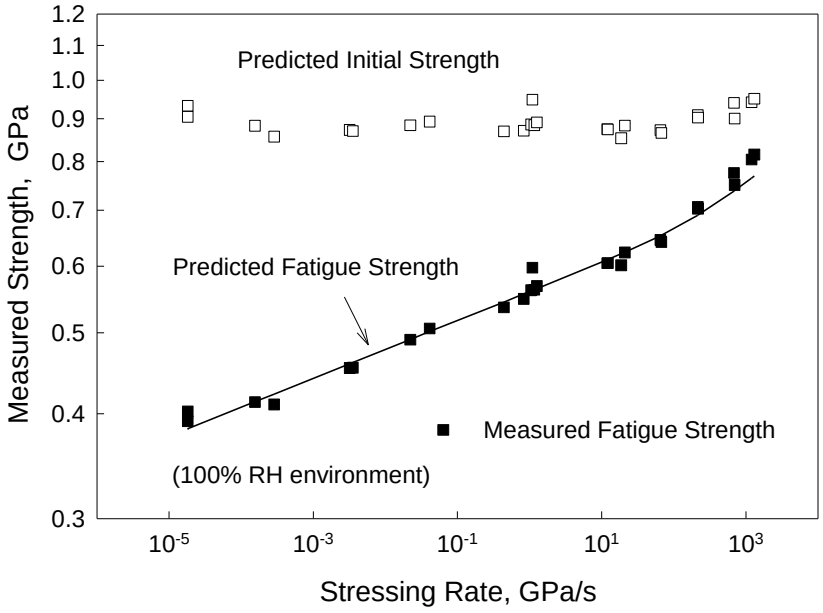

Figure 5b. Predicted Initial and Fatigue Strength for Abraded Optical Fiber Tested in 100% RH.

DISCUSSION

The predicted fatigue strengths reflect the measured strengths reasonably well, but do not show the degree of curvature observed in the data. At the faster stressing rates the predicted fatigue strengths underestimate the measured values. At the slow rates the slope of the predicted ambient curve yields a higher n_1 (28) than what one would determine by linear regression of the slowest rates alone (25). A better prediction of the measured data can be accomplished by an alteration to the model. This will be discussed later. Finally, there is clear non-power law curvature at the slowest stressing rates in the 100% RH environment. This curvature has also been reported for as-drawn fiber tested in a saturated environment at slow stressing rates.[10]

Figure 6 shows the predicted crack velocity curves for the crack growth parameters in Table 1 along with the crack velocity curves on bulk optical grade silica by Hibino et al.[11] The predicted crack velocities curves for optical fiber are in the range of the bulk silica data. The transition from region I to region II for optical fiber is nearly identical to that for bulk silica. The dependence of crack velocity on relative humidity is nearly the same as well. The n values for both crack velocity regions is lower for optical fiber than for the bulk silica.

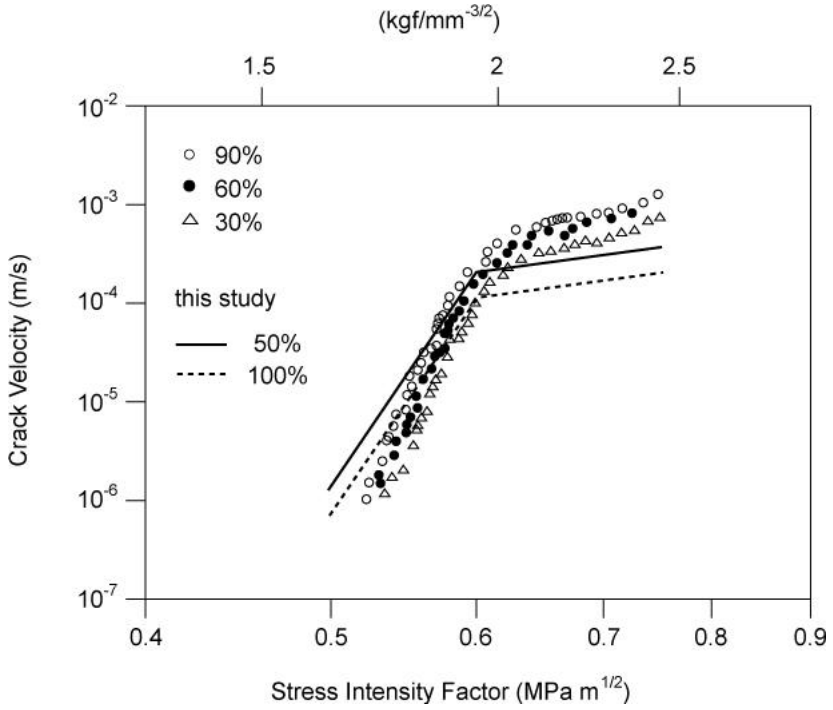

Figure 6. Predicted K-V Diagrams from the Abraded Fiber Data in Table I. Crack Velocity Measurements on Fused Silica for a Range of Humidity Levels by Hibino et al.[11]

Semjonov and Bubnov[12] have suggested altering the multi-region crack velocity model for optical fiber as shown in Figure 7. They cite the fact that many high-speed studies on optical fiber show the measured strength to be weakly dependent on stressing rate at intermediate stressing rates. The predicted strengths using their modified crack velocity model are shown in Figure 8 and provide an improved representation of the measured strength data at the extreme stressing rates. Note the intermediate stressing rate region on the predicted curves where the slope goes to zero. The region I n values are now closer to typical values of 20 to 25 found on optical fiber and are lower than those in Table I for the initial multi-region analysis. This compares with preliminary results on the same abraded optical fiber with the coating removed by hot concentrated sulfuric acid[13] where an n_1 value of approximately 24 was measured.

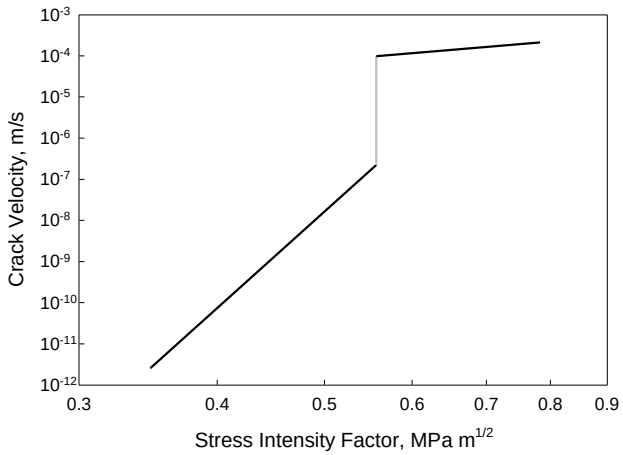

Figure 7. Kinked Crack Velocity Model Used By Semjonov and Bubnov to Model Dynamic Fatigue Behavior of High Speed Optical Fiber Tests.

Clearly a physical interpretation of the model in Figure 7 is lacking at this time, however, it is extremely useful from an engineering point of view. Since the dynamic fatigue data covers the range of typical stressing rate events during fiber processing, one models these events through interpolation rather than extrapolation. Therefore, a good fit to the data suffices for such modeling.

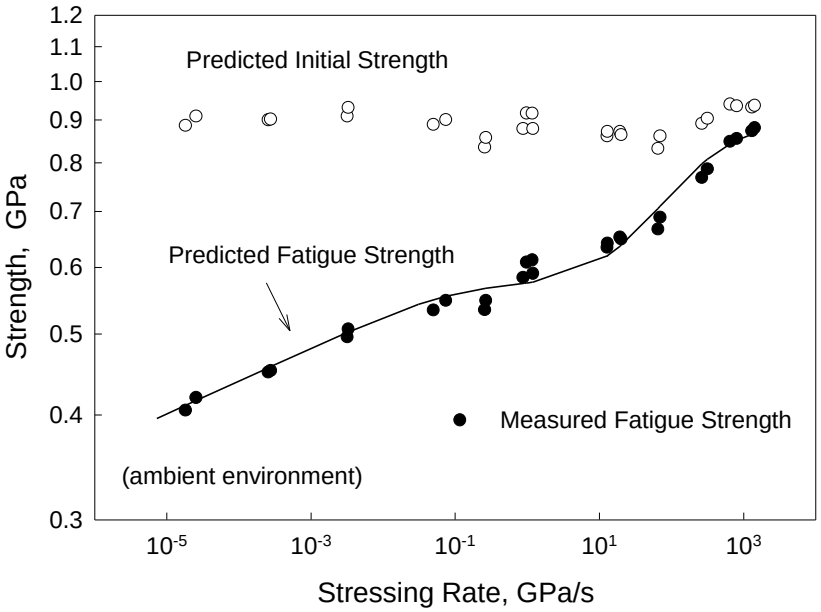

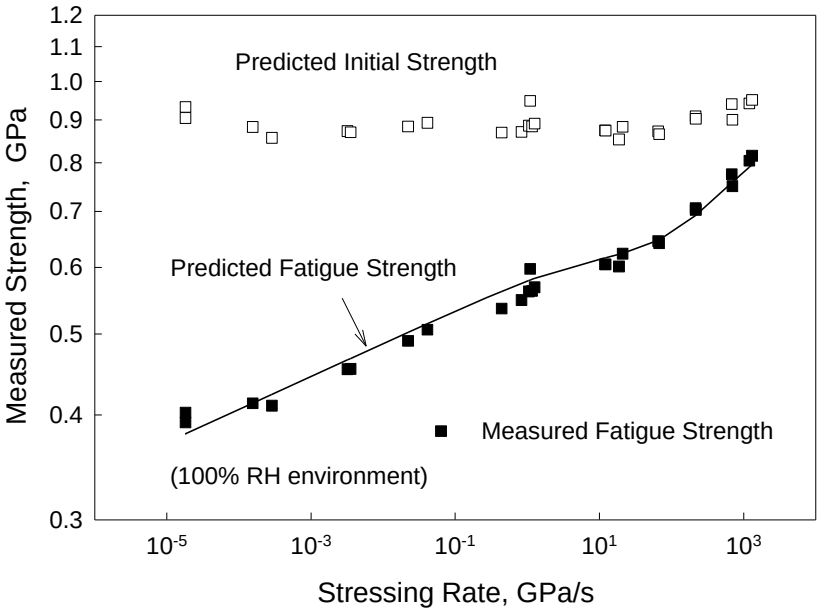

Figure 8. Dynamic Fatigue Predictions Using the Kinked Crack Velocity Model by Semjonov and Bubnov[12].

The presence of region II type crack growth has not been observed on high speed dynamic fatigue studies on soda-lime glass.[3,4] Chandan et al.[3] suggested that water has easier access to the smaller flaws tested in the dynamic fatigue study as compared to the large flaws in bulk glass studies. A transport limiting phenomenon does not occur as readily for such specimens. Proof test level flaws in optical fiber are several orders of magnitude smaller than those tested in the soda-lime glass studies; and therefore, one would expect no region II behavior for the flaws in this study based Chandan's hypothesis. Perhaps high-speed studies of abraded optical fibers without the polymer coating will yield further understanding in this area.

CONCLUSIONS

Proof stress level flaws in optical fiber were strength tested in a fatigue environment. Curvature in the dynamic fatigue plots was clearly evident at the higher speeds. The presence of region II type crack growth was put forth to explain the curvature and a multi-region crack growth model was used to deduce power law crack velocity parameters. Predicted crack velocity curves compared favorably to crack velocity measurements in high-purity fused silica. Regardless of the actual mechanism at these high speeds, it is important that engineers account for this behavior when modeling high-speed stress events commonly found during proof testing, cabling and installation of optical fiber.

ACKNOWLEDGMENTS

The critical review of S. Semjonov was much appreciated.

REFERENCES

1. T.A. Hanson and G.S. Glaesemann, J. Mater. Sci. **32** 5305-5311 (1997).
2. G.S. Glaesemann, Proc. SPIE, 2611, 38-44 (1995).
3. H.C. Chandan, R.C. Bradt, and G.E. Rindone, J. Am. Ceram. Soc., **61** [5-6] 207-210 (1978).
4. D.H. Roach, J. Am. Ceram. Soc., **69** [8] C-168 - C-169 (1986).
5. G.S. Glaesemann, pp. 689-704 in proceedings of the 41st International Wire and Cable Symposium, Reno, Nevada, November, 1992.
6. P.T. Garvey, T.A. Hanson, M.G. Estep, G.S. Glaesemann, pp. 883-887 in proceedings of the 46th International Wire and Cable Symposium, Philadelphia, Pennsylvania, November 1997.

7. E.R. Fuller Jr., S.M. Wiederhorn, J.E. Ritter, Jr., and P.B. Oats, J. Mater. Sci., **15** 2282-2295 (1980).
8. S.M. Wiederhorn, J. Am. Ceram. Soc., **52** [27] 99-105 (1969).
9. G.S. Glaesemann, K. Jakus, and J.E. Ritter, Jr., J. Am. Ceram. Soc., **70** [6] 441-444 (1987).
10. G.S. Glaesemann, pp. 297-307 in Proc. 10th NFOEC, Volume 4, San Diego, CA, June 1994.
11. Y. Hibino, S. Sakaguchi, and Y Tajima, J. Am. Ceram. Soc., **67** [1] 64-68 (1984).
12. S.L. Semjonov and M.M. Bubnov, Proc. of 1998 MRS Spring Meeting, San Francisco, CA, 1998.
13. M.J. Matthewson, C.R. Kurkjian, and J.R. Hamblin, J. Light. Tech., **15** [3] 490-497 (1997).